Received: 31 July 2023 | Revised: 15 November 2023 | Accepted: 11 December 2023

DOI: 10.1002/dro2.108

RESEARCH ARTICLE

Droplet WILEY

Actuating droplets with electrowetting: Force and dynamics

Robert Hennig[1] | Vito Cacucciolo[2] | Herbert Shea[1]

[1]Soft Transducers Laboratory (LMTS), Ecole Polytechnique Fédérale de Lausanne (EPFL), Neuchatel, Switzerland

[2]Politecnico di Bari, Bari, Italy

Correspondence
Herbert Shea, Soft Transducers Laboratory (LMTS), Ecole Polytechnique Fédérale de Lausanne (EPFL), Neuchatel 2000, Switzerland.
Email: herbert.shea@epfl.ch

Funding information
Swiss National Science Foundation (SNSF), Grant/Award Number: 200020_184661

Abstract

Electrowetting on dielectric (EWOD) allows rapid movement of liquid droplets on a smooth surface, with applications ranging from lab-on-chip devices to micro-actuators. The in-plane force on a droplet is a key indicator of EWOD performance. This force has been extensively modeled but few direct experimental measurements are reported. We study the EWOD force on a droplet using two setups that allow, for the first time, the simultaneous measurement of force and contact angle, while imaging the droplet shape at 6000 frames/s. For several liquids and surfaces, we observe that the force saturates at a voltage of approximately 150 V. Application of voltages of up 2 kV, that is, 10 times higher than is typical, does not significantly increase forces beyond the saturation point. However, we observe that the transient dynamics, localized at the front contact line, do not show saturation with voltage. At the higher voltages, the initial front contact line speed continues to increase, the front contact angle temporarily becomes near zero, creating a thin liquid film, and capillary waves form at the liquid–air interface. When the localized EWOD forces at the contact line exceed the capillary forces, projectile droplets form. Increasing surface tension allows for higher droplet forces, which we demonstrate with mercury.

INTRODUCTION

Electrowetting on a dielectric (EWOD) uses electric fields to control the shape and motion of droplets on solid insulating surfaces. The EWOD mechanism enables fabrication of solid-state fluidic devices: liquid droplets are the only moving parts, in contrast to systems using mechanical pumps or valves. Tunable liquid lenses and optical displays have been reported, using EWOD to control the droplet contact angles, while keeping the droplet in place.[1–4] Other applications use multiple EWOD electrodes to displace droplets. In digital microfluidics, individual droplets are displaced, merged, and split on a two-dimensional (2D) surface.[2,5–7] Digital microfluidic devices are highly reconfigurable, thanks to the absence of microfluidic channels. Several obstacles to commercialization, such as the need for high voltages and the presence of droplet traces have been investigated and addressed, enabling a recent transition of EWOD technologies from lab to industry.[2] Beyond digital microfluidics, the ability to apply forces on liquid droplets through electric fields makes EWOD a promising mechanism for microactuators based on liquid motion. Examples include the use of EWOD in micropumps and liquid micro motors and actuators.[8–12] Kedzierski and Holihan[13] and Kedzierski and Chea[14] recently reported rotational and linear actuators based on EWOD that achieve power densities comparable with those of high-performance electric motors.

We identified three aspects of EWOD that require further investigation: (i) the EWOD contact angle saturation with voltage, (ii) the derivations and measurements of the EWOD force acting on a droplet, and (iii) the transient dynamics of droplets. We discuss below

the state of the art of each of these topics and our contributions in this work to improve our understanding of them. Progress on these three aspects will improve the performance of EWOD devices, especially in devices where both droplet force and motion are needed, such as in pumps.

Contact angle saturation: In most EWOD experiments, an electrically conductive liquid droplet (e.g., water or an ionic liquid) is placed on a flat rigid substrate. The substrate consists of one electrode, covered with a typically 0.1–10 μm thick insulating dielectric layer. If the dielectric layer is not intrinsically hydrophobic, a thin top hydrophobic film is added to ensure initial high contact angles of the droplet. The contact angle is measured between the liquid meniscus and the substrate at the three-phase boundary where the liquid, gas, and solid intersect (see Figure 1a1,b1). When a voltage is applied between the droplet and the electrode, the electric field induces a decrease of the apparent contact angle, which is one of the most widely studied phenomena in EWOD.[17] We refer to the "apparent contact angle" rather than simply the "contact angle," because very close to the surface (typically within the order of a few microns), the contact angle does not change.[18] When observing the droplet, one generally only measures the apparent contact angle optically. We therefore refer to the "apparent contact angle" as the "contact angle" throughout this manuscript. The Young–Lippmann (Y–L) equation predicts a decrease of the apparent contact angle with the voltage squared[19]:

$$\cos\theta - \cos\theta_0 = \gamma_{LG}\frac{\varepsilon_0\varepsilon_r V^2}{2d}, \tag{1}$$

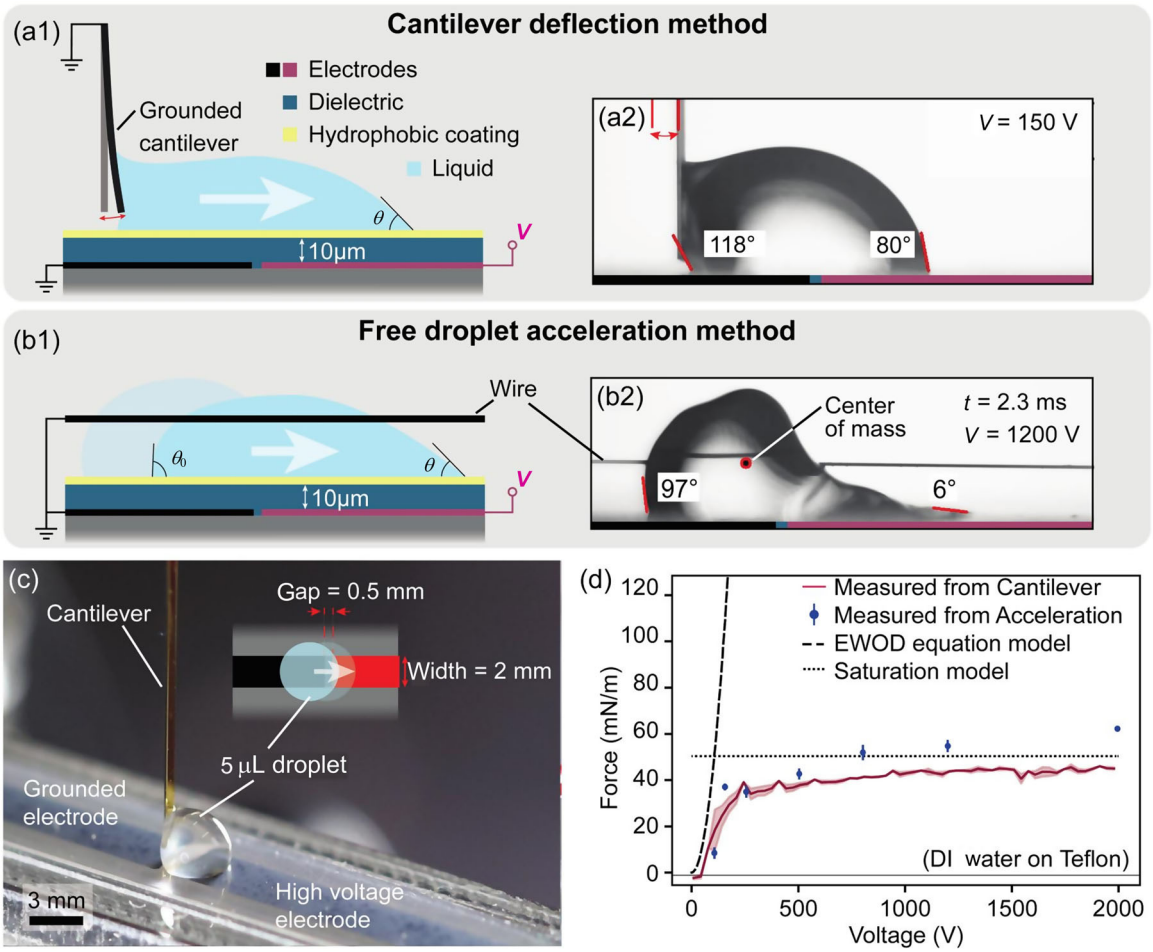

FIGURE 1 We use two setups to measure the electrowetting on a dielectric (EWOD) force and droplet dynamics: (a) the cantilever deflection method and (b) the droplet acceleration method. A 5 μL grounded droplet is placed such that it bridges the two electrodes, which are covered by a dielectric. The droplet moves to the right when a sufficiently high voltage is applied to the right electrode. The droplet shape and contact angle are measured using image processing on video taken at 6000 fps (Details in the methods section). (a) In the cantilever deflection method, the droplet adheres to the cantilever, and one determines the EWOD force from the cantilever deflection. (b) The free droplet acceleration method allows the droplet to move freely along a grounded wire. Multiplying the droplet's center of mass acceleration by the droplet mass allows computation of the EWOD force. At voltages far above the saturation threshold, we temporarily observed near-zero contact angles and very thin liquid films. (c) Photograph of the cantilever deflection setup. (d) The measured force, normalized over actuation width, as a function of the applied voltage to the right electrode. Both measurement methods show force saturation at around 50 mN/m, which agrees with the saturation force found in the literature.[15,16]

where θ is the contact angle at the applied voltage V, θ_0 is the initial contact angle at zero Volts, γ_{LG} is the liquid gas surface tension, ε_r is the relative permittivity of the dielectric, ε_0 is the vacuum permittivity, and d is the dielectric thickness.

Many groups have reported the saturation of the contact angle saturation with voltage: above a voltage threshold, the contact angle ceases to decrease. For example, deionized (DI) water on Teflon decreases from its initial contact angle of $\theta_0 = 115°$ to $\theta_{min} = 72°$ at 120 V (dielectric: 800 nm thick Teflon film)[20]; further increasing the voltage does not further decrease the equilibrium contact angle.[18,19] While the cause of contact angle saturation is still not fully understood, the Young–Lippmann equation, which does not predict contact angle saturation, likely fails because two assumptions made at low voltages do not hold at high voltages.[18]

First, the Y–L model assumes a perfectly insulating dielectric layer and surrounding air. The commonly used dielectrics, such as amorphous fluoropolymers (e.g., Teflon) contain trapped charges whose density and sign depend on the history of the applied electric field.[20–23] By applying suitable modulated bipolar alternating voltages to minimize dielectric charging, the minimum contact angle of DI water has been reduced from 72° to 65°.[21]

Second, the Y–L equation and most other EWOD models are 2D models. However, at high voltages, transverse instabilities of the contact line break this assumption.[18] Early experiments by Vallet et al.[24] reported projectile droplets separating from the main droplet at voltages beyond saturation, similar to mechanically shaken droplets.[25] In contrast to the imperfect insulator properties, the geometric instabilities have been less explored. However, they are of similar fundamental interest as charge trapping for EWOD saturation and could find applications like microfluidic droplet generation.[26]

EWOD force: The setups that we report here are designed to move the center of mass of droplets and are, therefore, similar to EWOD digital microfluidics and EWOD actuators. The droplet is not initially centered over a single electrode but bridges two. Application of a voltage to the right electrode, while the left electrode and the droplet are grounded, causes the right side of the droplet to experience a force and hence a contact angle decrease, but not the left side (Figure 1a). A resulting net force causes the droplet to move toward the actuated electrode. There exist extensive theoretical derivations on this force, for which we summarize the main three models below.[3,19] They all result in the following equation:

$$F_{EWOD} = w\frac{\varepsilon_0\varepsilon_r V^2}{2d}, \tag{2}$$

where w is the projected droplet width on the electrode perpendicular to the direction of motion. The EWOD force is often normalized by the droplet actuation width as $f = \frac{F_{EWOD}}{w}$.

In the first of the three models, the electromechanical EWOD model, one considers an electrostatic pressure acting on the surface of the droplet. As a voltage is applied between the droplet and the electrode, accumulated charges near the triple contact line of the droplet result in a localized force. This EWOD force moves the contact line and changes the apparent contact angle. The electromechanical EWOD model was verified by Mugele and Buehrle.[18,19,27] They estimate that the force on the droplet edge is significant within a distance d from the rigid surface, with d being comparable to the thickness of the dielectric layer.

In the second model, one considers the change of capacitive energy stored in the system, as the droplet slides over the electrode.[19,28] This approach leads directly to Equation (2).

In the third model, droplet mechanics predict the force F_{CA} on a droplet in relation to its front and rear apparent contact angles θ_f, θ_r as given by[17,19,29]

$$F_{CA} = w\gamma_{LG}(\cos\theta_f - \cos\theta_r). \tag{3}$$

Equations (3) and (2) are equivalent if we assume the difference between front and rear contact angle to follow the Young–Lippmann Equation (1). The EWOD actuation force is not necessarily a consequence of the observed contact angle difference, as Equation (3) may suggest. Experiments have shown EWOD forces without a change in contact angle.[17,28,30]

Similar to contact angle saturation with voltage, a saturation of the EWOD force with voltage has been experimentally observed, in contradiction with Equation (2). The force saturation has been reported for instance in capillary rise experiments, in which a liquid is pulled up between two dielectric-coated electrodes using EWOD.[11,15,28,31,32] The liquid height can be considered equivalent to a pressure. Ni et al.[16] measured the EWOD force on a droplet by confining the droplet beneath a flat plate and measuring the force on the plate.[33] They observed that force saturation occurs at lower voltages and reaches lower maximum forces if one adds surfactants to water, which reduces the surface tension and initial contact angle. In their force measurement setup, the contact angle cannot be measured because the drop is squeezed under a flat plate. No other direct EWOD droplet force measurements have been reported, despite its importance for confirming theoretical predictions and for applications.

Transient dynamics: The EWOD electrostatic forces act against inertial forces and drag forces. Drag forces mostly take place at the contact line, which is observable through contact angle hysteresis.[34–36]

The transient behavior of an EWOD-actuated droplet can be divided into two regimes.[37–39] Depending on the droplet size, droplet viscosity, and the applied voltage, the droplet is either overdamped, meaning that it slowly transitions to the equilibrium shape and position or it is underdamped, meaning that it deforms beyond the equilibrium shape before returning to that equilibrium. Vo and Tran[40] recently investigated application of voltages higher than contact angle saturation in a highly underdamped situation. They observed strong capillary waves and found that the initial contact-line velocity increases even at voltages where contact angle saturation is observed. They did not measure the transient contact angle. An understanding of droplet dynamics is required, for example, when increasing digital microfluidic speeds or in applications in which droplets jump.[41–43]

Measurement setups for EWOD force: Here, we present two measurement setups that directly measure the EOWD force on droplets while concurrently recording the contact angle and possible droplet emission at a high framerate (6000 fps), enabling analysis of dynamic behavior. For both setups, we place a grounded 5 μL droplet on a hydrophobic surface such that it bridges two insulated electrodes (Figure 1a,b). Application of a voltage on the right electrode, while keeping the left electrode grounded, pulls the droplet toward the right electrode. The "cantilever deflection" method attaches a droplet to a cantilever and computes the EWOD force from the cantilever deflection (Figure 1a,c). This method is the first to measure simultaneously the force and contact angles of a single droplet. The "free acceleration" method allows the droplet to move freely and tracks its center of mass. The EWOD force is calculated by multiplying the droplet's acceleration by its mass (Figure 1b).

We validate the measurement methods by comparing them with each other. Further, we show that for most cases, Equation (3), which is based on the current contact angles, predicts the measured force well. All measurements show a force saturation with voltage (Figure 1d) and only slight increases in force beyond the saturation voltage. We measured the highest reported EWOD force per actuation width with the higher surface tension droplet Mercury at 100 mN/m. Transient dynamics during actuation (duration of around 15 ms) show that EWOD forces are concentrated at the contact line and can temporarily result in spreading of a thin liquid film with effective zero contact angle, generating strong capillary waves and ejecting satellite droplets. The zero contact angle and fast advancing front contact line are in apparent contradiction with the observed overall force saturation. Our observations show that the transient driving force at the front contact line can increase significantly beyond the saturation force.

RESULTS AND DISCUSSION

Free acceleration method: Qualitative dynamics: In the free acceleration method, we apply a voltage step to the right electrode and observe the droplet accelerating toward the right. The method resembles applications like digital microfluidics, where the droplet accelerates and moves with little drag. We divide the droplet response into three characteristic phases, as shown in Figure 2, which contrasts behavior at 100 V and at 1200 V.

Phase (1). The first phase starts when we apply a step DC voltage. For an applied voltage of 100 V, the front contact angle, the one located on the actuated electrode, decreases from over 100° to 60° within less than 1 ms. The front contact line advances less than 1 mm within 6.7 ms. For a step voltage of 1200 V, the front contact angle decreases from over 100° to 10°, well below the expected saturation angle of 60°, in less than 1 ms. The front contact line advances by 3.2 mm within 6.7 ms. This corresponds to a droplet length increase of 155%, compared to 42% at 100 V. The fast motion of the front contact line results in a thin film with near-zero contact angle spreading over the 1200 V electrode. For both levels of applied voltage, the rear 80% of the droplet does not move at all. A capillary wave, a wave between the interface of water and air, travels from the front of the droplet to the rear.

Phase (2). The second phase starts when the capillary wave reaches the rear of the droplet (see Figure 2a3,b3, at 6.7 ms). This is the main acceleration phase of the droplet as its center of mass moves toward the actuated electrode and its speed increases (Figure 2d). The capillary wave causes the rear contact line to initially move slightly backward before moving forward. The rear contact angle decreases as the droplet moves forward due to contact angle hysteresis, but not as much as the front contact angle, which is directly over the actuated electrode (Figure 2g). At 1200 V, the front contact point accelerates faster than the bulk of the droplet. As the thin liquid film spreads, it breaks up and small droplets separate from the main droplet (projectile droplets, Figure 2a4). The emission of projectile droplets causes the front contact angle of the main droplet to increase.

Phase (3). The third phase starts when the rear contact point of the droplet reaches the actuated electrode, that is, when the droplet is entirely over the actuated electrode and hence when EWOD force is no longer applied to the droplet. The rear contact angle decreases to a value lower than the front contact angle. The droplet decelerates and eventually stops moving. The droplet actuated at 1200 V moves outside of the field of view.

The droplet actuated at 100 V behaves in good agreement with established EWOD theory.[34,44,45] The front contact angle decreases to the minimum saturation angle of around 60° as the droplet moves forward. The rear contact angle decreases slightly as the contact line starts moving, which is well-known as contact angle hysteresis.[46] Using Equation (2), we can predict the droplet force based on the front and rear contact angles (Figure 2h). The force from the contact angle difference agrees within the margin of error with the force determined from the acceleration during transient behavior at 100 V.

The droplet behavior at 1200 V suggests that saturation at the droplet front contact line can be avoided for timescales of up to 10 ms. A similar time delay of saturation was demonstrated by Li et al.[21] for contact angles, by Vo and Tran[40] for transient contact line speed, and by Wang and Jones[31] for capillary rise experiments. However, this delay of saturation has not previously been investigated in detail and has not been studied for voltages over 700 V. We observe near-zero contact angle and a rapidly spreading droplet for over 10 ms. One explanation could be that trapped charges, a cause of saturation, do not form immediately in the dielectric. Li et al.[21] explained their delay of saturation with this delay in trapped charges. For our case, the front droplet edge appears to move faster than charges accumulate, so the front droplet edge constantly reaches the new dielectric surface, where charges are not yet trapped. This may cause an extended period of no saturation. Cases where the interface moves faster than the bulk liquid find applications in high-speed switches and have been previously studied.[47,48]

We observe that the droplet movement is clearly initiated from the very front tip of the droplet. This fits well with the

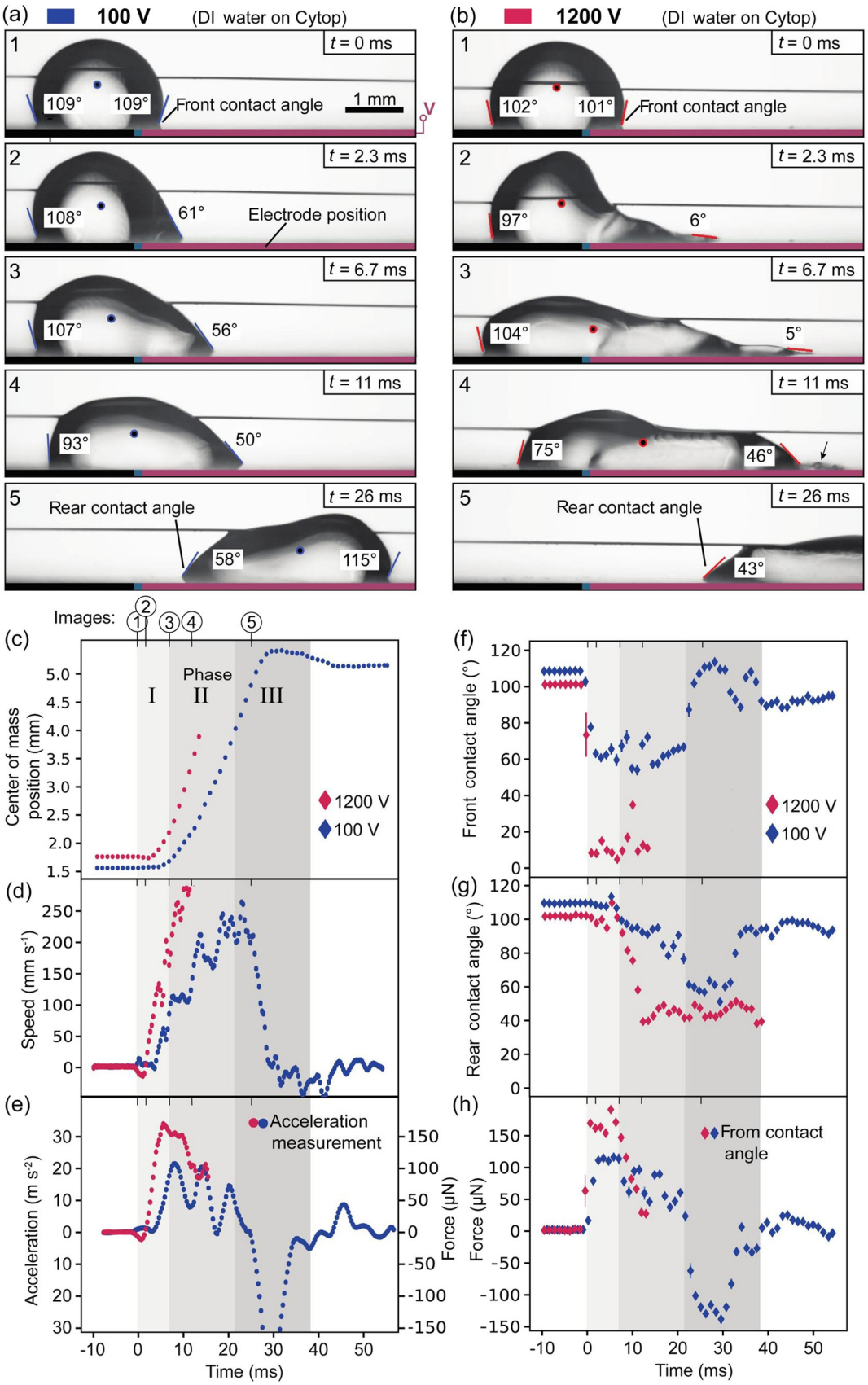

FIGURE 2 (See caption on next page).

electromechanical EWOD model, where an electrostatic force acts on charges concentrated in the front contact line of the droplet.[28,36,49] This localized point force at the front contact line does not seem to saturate with increasing voltages. The absence of saturation at the front edge is backed up by the decrease to a near-zero contact angle and the rapid spreading of the thin liquid film. Unlike for a rigid object, which moves but does not deform when a force is applied, the localized EWOD force has strong effects on the shape of the droplet. With increasing voltages, the droplet increasingly stretches as the rear part of the droplet accelerates more slowly. We also observe capillary waves, and projectile droplets that separate from the main droplet. Our high-speed videos show the formation of projectile droplets, from an initial spreading liquid film, to a bulge, to the separation from the main droplet. Vallet et al.[24] and Mugele and Herminghaus[50] previously reported the existence of projectile droplets at high voltages (around 1000 V). We hypothesize that projectile droplets form when the EWOD point force at the front line exceeds the surface tension, which holds the droplet together.

Free acceleration method: Quantitative dynamics: The droplet spreading occurs primarily in the inertial regime. This is consistent with the very low Ohnesorge number of 0.0023 for our droplets. The observed capillary waves are also an indicator of being in the inertial regime. We analyze the front edge position using spreading exponents, which are commonly used in spreading dynamics research. Similar to Du et al.,[51] we use the equation $\frac{r_f}{r_0} = C\left(\frac{t}{\tau_i}\right)^{\alpha}$ with $\tau_i = \sqrt[2]{\frac{\rho r_0^3}{\gamma}}$ where r_f is the front droplet position, r_0 is the initial droplet radius, t is the time, τ_i is a rescaling inertial-capillary time, and ρ is the density.

For our experiments, τ_i equals 10.5 ms. The spreading coefficient C and exponent α are fitted to our experimental data (details shown in Supporting Information: Figure S1). In Figure 3a,b, we plot the spreading exponent and coefficient versus the voltage. The coefficient C increases with increasing voltages. At low voltages, the exponent α equals around 1, so the spreading over time is mostly linear. As we increase the voltage, we observe lower exponents down to 0.36, which is comparable to the spreading observed when wetting a smooth surface.[51]

In Figure 3c, we plot the measured speed of the front contact line during the first 8 ms after applying the step voltage. The aim is to observe the front edge speed with minimum effect from the rear bulk of the droplet. We chose 8 ms as it is the highest time when the front edge continues to accelerate. For longer times, the rear bulk increasingly slows further spreading and projectile droplets form. We observe that the velocity keeps increasing significantly beyond saturation voltage, which is consistent with our prior observation that the localized force on the font contact line does not saturate. This

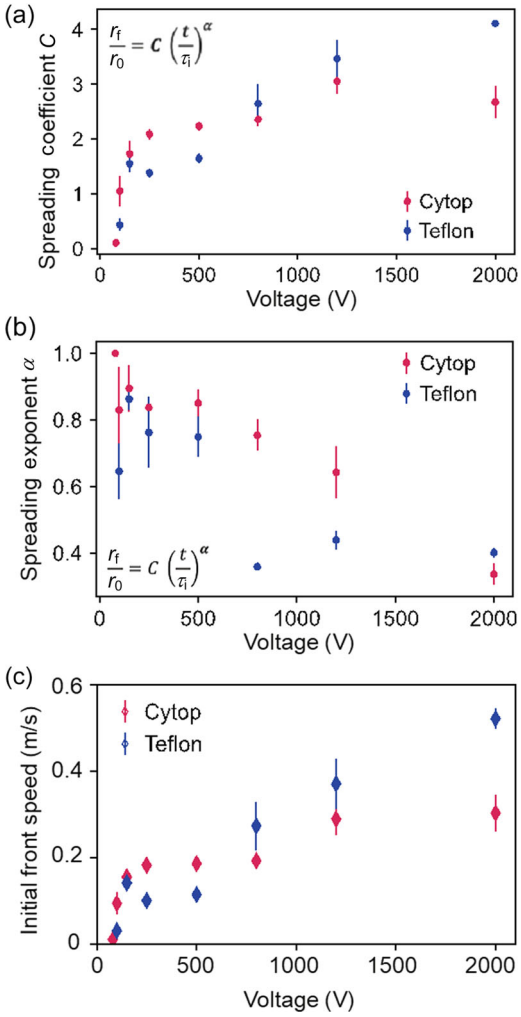

FIGURE 3 The spreading coefficient C, exponent α, and droplet front speed versus voltage. Each marker represents three measurements. (a, b) Fitting the initial spreading of the front contact line to a general spreading equation yields coefficient C and exponent α. (c) Speed of the front contact line as measured during the initial 8 ms of applying the step voltage. The initial front speed continues to increase, even at high voltages.

FIGURE 2 "Free acceleration" method to measure electrowetting on a dielectric (EWOD) force and dynamics. (a) and (b): video frames of a deionized (DI) water droplet moving on a Cytop coating during EWOD actuation at two different voltages. The voltage step is applied at $t = 0$ ms. (a) On applying a step voltage of 100 V to the right electrode, the front contact angle decreases and the droplet moves toward the actuated electrode. (b) On applying 1200 V, the front contact angle becomes near zero as the thin liquid film advances rapidly. The arrow on the right side of b4 points out projectile droplets. (c–e) The position of the center of mass of the droplet is tracked over time. The first and second derivatives of position provide speed and acceleration versus time. We divide the droplet movement into three phases. In the first phase, only the front contact line moves. In the second phase, the entire droplet accelerates. In the third phase, the droplet decelerates. (f) Front (right) contact angle versus time. The contact angle responds in less than a millisecond to the applied voltage. For 1200 V, the angle reduces to near zero, far below the saturation angle. (g) Rear (left) contact angle versus time. (h) Force determined using Equation (2) and the contact angles. The modeled forces are similar to forces determined from droplet acceleration in (e).

observation agrees with Vo and Tran,[40] who observe a similar absence of saturation and confirms the trend at higher voltages.

Free acceleration method: Force measurements: Using the free droplet acceleration method, we measure (i) the EWOD force, (ii) the contact angles, and (iii) the initial speed, for step voltages of up to 2000 V. The droplet force versus voltage is plotted in Figure 4a. The force is determined by multiplying the droplet acceleration with the droplet mass (Details in Supporting Information: Figure S2). We consider the acceleration as taking place from the moment the voltage is applied until the moment the droplet fully covers the actuated electrode.

As can be seen in Figure 4, the difference in EWOD force between Teflon and Cytop coatings is negligible. Up to 150 V, the force increases to 50 mN/m and then nearly saturates, reaching 75 mN/m at 2000 V. The force values are similar to those obtained by other groups: Ni et al.[16] reported 46 mN/m maximum force for water in oil, and Wang et al.[45] reported 33 mN/m for water in air (see Supporting Information: Table S1). The 50% increase in force from around 150 V up to the maximum 2000 V from the droplet acceleration method is in contrast with the cantilever deflection method, where we measure no further increase for higher voltages. We hypothesize the dynamics at the front edge of the droplet to be responsible. The two methods differ in dynamics: in the cantilever method, the droplet is static, while in the droplet acceleration method, the droplet moves at high speed.

In Figure 4b, we use Equation (3) to calculate the EWOD force based on the average contact angle difference. Compared to the force determined from acceleration shown in Figure 4a, the variance is larger, but the force values and saturation shape are in very good agreement. The quadratic voltage model in Equation (2) predicts a more than 170-fold increase in EWOD force between 150 V and 2000 V, which is in stark contrast with the 1.5x increase that we observe (Figure 4a).

Cantilever deflection method: Force: In the cantilever deflection method, where a cantilever is pulled by the droplet, we ramp up the DC voltage over 8 s from 0 V to 2000 V. The voltage ramp (rather than a step) serves to minimize dynamic effects. The voltage, contact angle, and force of a representative example of DI water on Teflon are shown versus time in Figure 5. In the initial 0.5 s, as the voltage reaches 120 V, the front contact angle decreases from an initial value of 125° to 80°. The force from the capillary deflection reaches approximately 100 µN. This measured force agrees well with the force computed from the contact angle difference using Equation (3). We do not observe any significant change in cantilever deflection or contact angles when increasing the voltage further from 120 V to 2000 V. Consequently, we find that the droplet force saturates even at 2 kV, in agreement with what we observed using the free droplet acceleration method. As the voltage is turned off, the droplet contact angles and cantilever deflection remain in the actuated configuration. In principle, EWOD is reversible: the force and contact angle return to their initial values when the voltage is turned off. Exceeding the saturation voltage probably caused significant charge trapping, leading to the observed non-reversibility of EWOD.

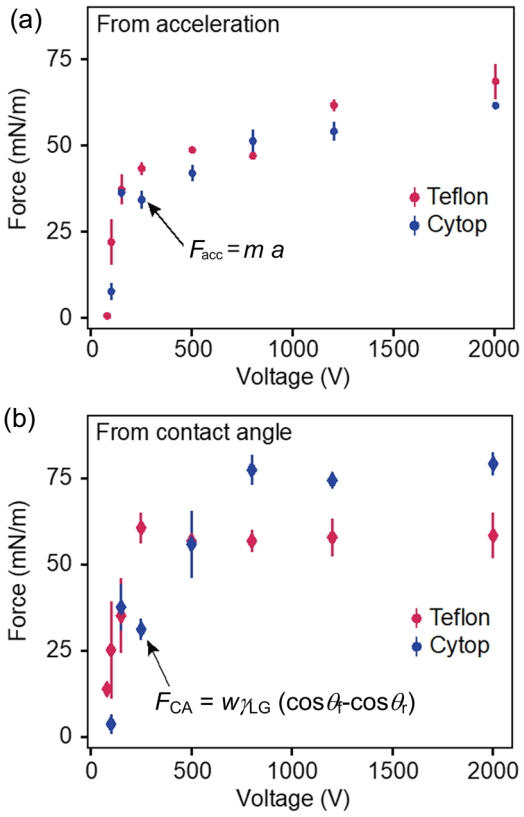

FIGURE 4 Electrowetting on a dielectric (EWOD) force versus voltage for a deionized (DI) water droplet in the free acceleration method. Each marker represents three measurements. (a) EWOD force versus applied voltage, determined by multiplying droplet acceleration by its mass. Differences between Teflon and Cytop are negligible. Saturation is observed near 150 V. (b) EWOD force computed from the contact angle difference (Equation 3). The magnitude of force and saturation shape strongly resemble the data in graph (a).

Using the cantilever deflection method and a voltage ramp, we can measure the EWOD force and contact angles up to high voltages and with negligible dynamic effects. This allows quantitative comparison between droplet liquids to better understand the effect of different surface tensions. We use an ionic liquid (EMI-(CF3SO2)2N), DI water, salt water (3 M), and pure mercury, chosen for their differences in surface tension and differences in chemical nature.

The droplet shapes before and during EWOD actuation for three liquids are shown in Figure 6, as are the forces from both the cantilever deflection measurement and the contact angle model.

Mercury has a high surface tension (435 mN/m). For mercury, the initial 144° contact angle changes by only 8° under high voltages. The force increases to 100 mN/m with no saturation until 2000 V, where the electrical breakdown limit of the dielectric was reached. For salt water and DI water, which behave very similarly to each other (both have a surface tension of 72 mN/m), the contact angle decreases by 42° and the forces saturate below 45 mN/m. For the ionic liquid, the initial contact angle of 73° decreases by 22°. The ionic liquid's lower surface tension (24 mN/m) results in lower forces

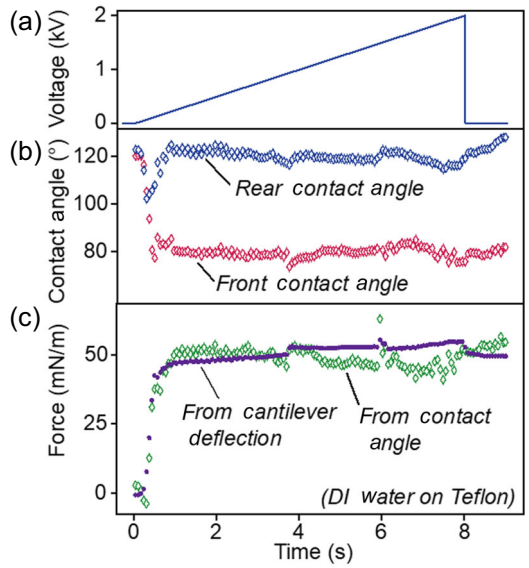

FIGURE 5 A representative example of data from the cantilever force method, plotted versus time. (a) The applied voltage is ramped up to 2000 V over 8 s. (b) The front contact angle decreases as the voltage increases, while the rear contact angle remains almost constant. (c) The force measured using the cantilever deflection and the force computed from a change in contact angles agree well with each other and show a clear force saturation at 50 mN/m after less than half a second, that is, at a voltage of 120 V.

than 20 mN/m. The ionic liquid detached from the cantilever at voltages above 800 V.

The forces computed from the contact angle model match the measured forces from the cantilever method within the margin of measurement errors, even under changing surface tensions and chemically different droplets. This underlines the general validity of Equation (3).

Equation (3) predicts a force that scales linearly with surface tension if the contact angle change remains the same. Our observations show a similar trend, even though the initial contact angle and contact angle reduction depend significantly on surface tension or droplet material. The trend of increasing maximum EWOD force with increasing surface tension can also be seen when comparing EWOD force experiments or actuators in the literature (see Supporting Information: Table S1). Across materials and setups, the force normalized over the actuation width seems to be limited by the value of the liquid surface tension. To verify this hypothesis, more experiments and theoretical models are needed. For example, the initial contact angle of the droplet could play a role in limiting EWOD forces.

The formation of projectile droplets: The formation of projectile droplets is not compatible with the hypothesis that the droplet is a single cohesive body whose shape can simply be described by the front and back contact angles. We experimentally investigated the formation of projectile droplets not only during the free acceleration method but also with the droplet pinned to the cantilever beam, where the bulk of the droplet mostly remains in place.

Figure 7 shows images of the formation of projectile droplets for DI Water on Teflon at 1475 V, taken at 6 ms intervals. The 80° front contact angle and 100 μN of cantilever force both remained unchanged after reaching saturation at 120 V. The projectile droplet formation is initiated by the front edge of the droplet locally flattening to form a thin liquid film with near-zero contact angle (Figure 7e2). This liquid film spreads over the actuated electrode. After 10 ms, as the film spreads beyond 1 mm, the thin film breaks up into small projectile droplets. The main droplet returns to its initial 80° contact angle (Figure 7e5). The phenomenon is concentrated at the front contact line apart from capillary waves, which travel to the back side of the droplet, causing oscillations in the rear contact angle and cantilever deflection force. Except for the oscillations, the measured force on the cantilever does not change (Figure 7d).

Our observations hint at a shift of balance between the electrical forces, localized at the front edge of the droplet, and the liquid surface tension, which holds the droplet together. At lower electric fields, surface tension dominates over electrical forces. The electrical forces are transmitted from the front edge to the main body of the droplet and cause changes in the contact angle, with the droplet shape remaining very similar. When the voltage far exceeds the saturation value, electrical forces become dominant at the front edge, first creating a discontinuity in the front contact angle with the formation of a thin film until the droplet breaks apart, as surface tension forces are no longer sufficient to maintain its cohesiveness.

CONCLUSION

The free acceleration method and the cantilever deflection method are complementary methods to observe both the force and the dynamics of EWOD actuated droplets. Both our methods provide similar quantitative and qualitative results, though one allows droplet motion and one strongly limits droplet displacement. The setups allow the study of quasi-static cases, as well as transient behavior that take the droplet out of the equilibrium conditions where the droplet can be described by the contact angles.

The EWOD forces that we measured with both our methods are similar to values reported in the literature (see Supporting Information: Table S1). We observe force saturation for DI water with both experimental methods, even at voltages of up to 2000 V. Consequently, when aiming to maximize forces in applications such as actuators or pumps, increasing the drive voltage beyond saturation (e.g., of order 200 V) is not helpful. High voltages create instabilities such as projectile droplets and do not lead to higher forces. Kedzierski and Holihan[13] and Kedzierski and Chea[14] maximized the actuation width, which linearly increases the force. The increased forces seen for higher surface tension liquids could be exploited, for instance, by using mercury. With mercury, we measured the highest reported EWOD force per actuation width of 100 mN/m, while for other liquids, reported DC forces are below 50 mN/m. Wang and Jones[15] use 5 kHz AC to achieve an 88 mN/m equivalent force with water in air. To investigate this increase in force, the measurement

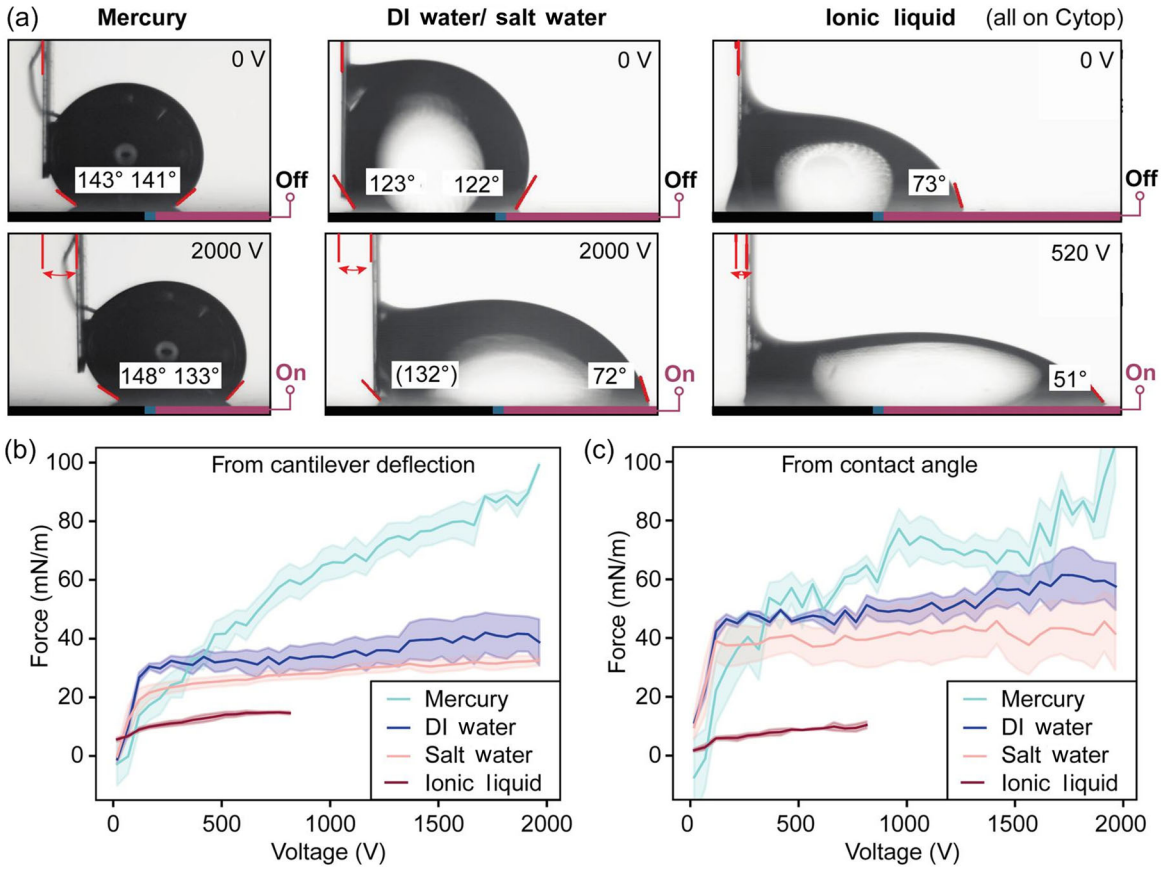

FIGURE 6 Images and EWOD force data from the cantilever deflection force method. The three liquids have the respective surface tensions: mercury (435 mN/m), water (72 mN/m), and an ionic liquid (24 mN/m), all on Cytop. (a) Images show a representative frame before and after applying a voltage. The force exerted by the droplet deforms the cantilever. (b) EWOD force was measured using the cantilever deflection versus voltage. The nonzero force at zero voltage for the ionic liquid is likely due to static friction. (c) EWOD force computed from the contact angle difference and Equation (3). Cantilever deflection and contact angle forces are in good agreement. The force saturation observed for deionized (DI) and salt water does not hold for mercury, which continues increasing in force until 2000 V. We observe higher maximum forces for liquids with higher surface tension.

methods that we report here could be expanded to using bipolar alternating voltages. Further expansions of this work could be to surround the droplet by oil or to use a parallel plate configuration, which is frequently used in applications for digital microfluidics.

We report transient dynamics of highly underdamped droplets at voltages up to 2000 V. We observe near-zero contact angles, thin liquid films, and strongly deformed droplet shapes, which are in contradiction with the classic understanding of EWOD, where a droplet is defined by its front and rear contact angles. The findings are in line with the electromechanical EWOD model, which explains the localized force that we observe at the front contact line of the droplet. Projectile droplets form when the local transient force at the droplet front edge exceeds the droplet's surface tension. Such contact line instabilities and the buildup of charges likely cause the droplet to return to the saturation contact angle at equilibrium. In addition to providing insights into EWOD contact angle and force saturation, the transient dynamic observations could find application in making droplets jump, purposefully creating projectile droplets or increasing droplet response speeds.[41–43]

METHODS

We use two setups; one for the free droplet acceleration method and one for the cantilever deflection method. In both setups, a 5 µL droplet is placed with a micropipette on the same sample, a flat rigid surface with two embedded electrodes. The rectangular electrodes are 0.5 mm apart and 2 mm wide, chosen to be smaller than the droplet diameter of around 2.5 mm. This ensures that the width over which the droplets are actuated remains at 2 mm throughout the experiments. A consistent width is important because the force depends linearly on it. The electrodes are patterned by etching the Al layer on a 125 µm thick aluminized PET base sheet (metalized Polyester Film; McMaster-Carr). We print the desired electrode shapes with a wax printer (Xerox ColorQube 8580) onto the aluminized PET and etch the aluminum, which is not covered by wax, in a 2% KOH solution in water. After removing the remaining wax with a laminator and paper, we blade-cast a 10 µm thick PVDF-TrFE-CTFE (Piezotech RT-TS) dielectric layer and cure at 100°C for 2 h. The PVDF is chosen for its high relative electric permittivity of 40

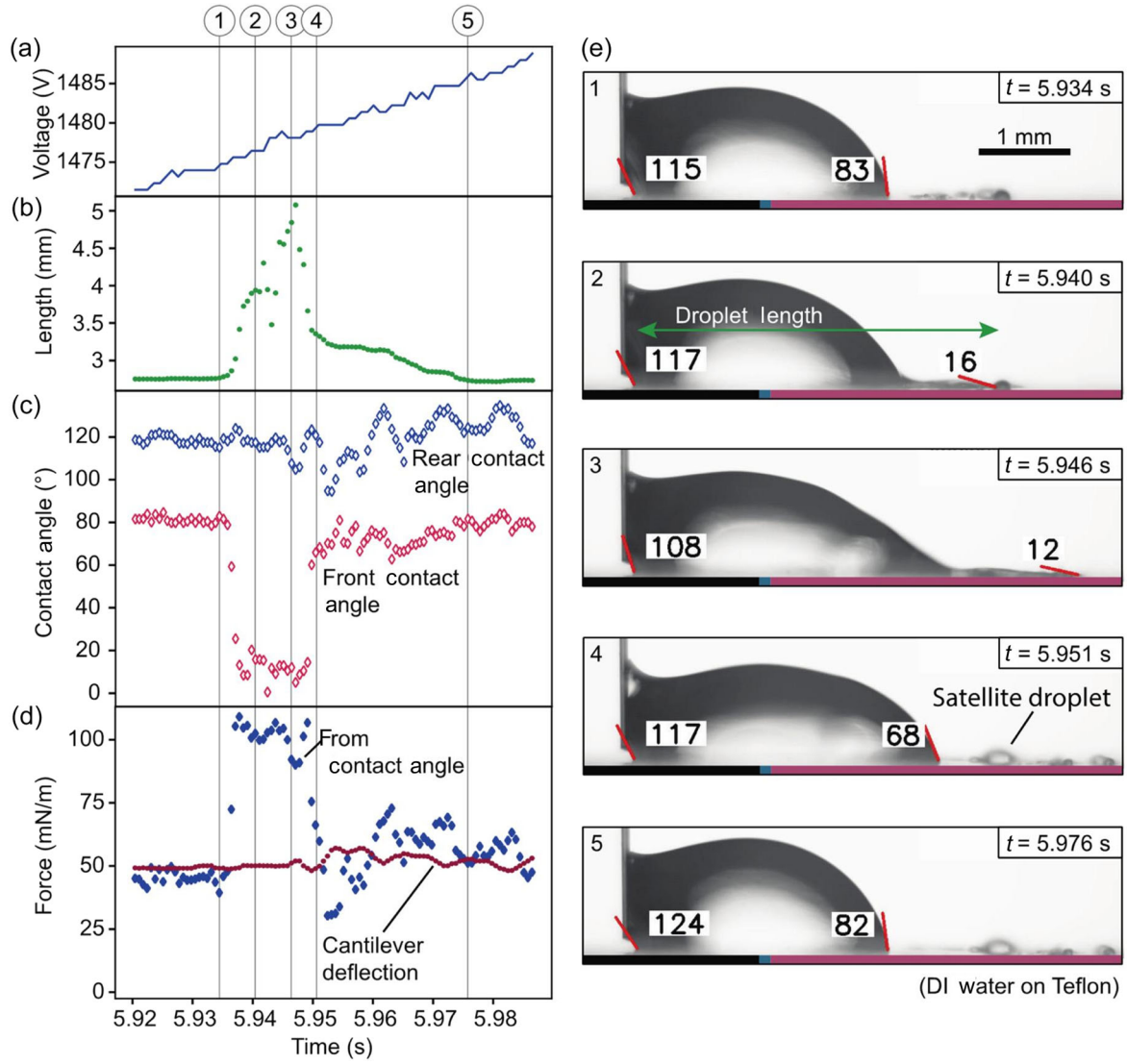

FIGURE 7 Formation of projectile droplets for the main droplet pinned to a cantilever beam. The figure shows a 30 ms window during the 8 s voltage increase up to 2000 V. (a) The voltage increases linearly as a function of time, from 1470 V to 1490 V. (b) The droplet length increases significantly due to the formation of a thin film of liquid at its front edge. The length then returns to its initial value when the film breaks apart into satellite droplets. (c) Front and rear contact angles versus time. The front contact angle decreases to near-zero degrees for 15 ms as part of the droplet deforms into a thin film, before returning to its initial value of 80°. (d) The force measured from the cantilever deflection and the force predicted by the contact angle model. While the cantilever force measurement does not show any significant variation, the contact angle model predicts a temporary force increase by 2x, due to the local decrease in the front contact angle when the thin film forms. (e 1–5) Frames taken with a high-speed camera, showing the satellite droplet formation. A thin liquid film forms at the front edge and spreads toward the rightmost positive electrode, until it breaks into satellite droplets.

and high breakdown strength of 300 V/µm.[52] The hydrophobic coating of either Cytop or Teflon is spin-coated at 3000 rpm for 30 s, resulting in a thickness of 1–1.5 µm. The coatings are commonly used in EWOD studies. After curing at 180° for 2 h, we rub the far end of the electrodes with acetone to expose them and make contacts.

Free droplet acceleration setup: To electrically ground the droplet, a 50 µm diameter wire runs through the droplet. The wire is parallel to the droplet motion direction to minimize drag. We estimate the maximum drag force as 11 µN, obtained by multiplying the water surface tension by the circumference of the wire. This drag force makes up less than 10% of the droplet force at low voltages. Starting from an all-grounded state, a voltage step from 100 V up to 2000 V is applied to the right electrode. The other electrode and droplet are grounded. A high-speed high-voltage amplifier (model Trek 10/10B-HS) is used to apply the high voltage. The amplifier can deliver sufficient current, such that 90% of the set voltage is reached in less than 0.13 ms, faster than the dynamics of the droplet.

Cantilever deflection setup: In the cantilever deflection method, we place a droplet at the bottom of a 30 mm long and 0.04 mm × 0.4 mm cantilever (0.028 mm wall thickness, by CM Scientific) (Figure 1c). The cantilever is sputter-coated with a chromium adhesion layer and gold. The conductive cantilever is used to ground

the droplet. For the mercury experiments, an additional copper wire grounds the droplet, as gold is dissolved by mercury. The droplet adheres to the cantilever due to surface tension. When the droplet experiences an EWOD force, it pulls the attached cantilever, deflecting the cantilever. This deflection allows us to determine the force (details on cantilever calibration given in Supporting Information: Figure S3). A similar setup was used by Gao et al.[53] to measure droplet–solid friction, but not in the context of actuating a droplet. The cantilever dimensions were chosen such that the area of contact with the droplet is large enough to avoid droplet detachment. For water, the contact area is around 1 mm^2, resulting in a detachment force of around 150 µN. The cantilever deflection should be large enough to be observable with the camera but small enough that the droplet keeps bridging the electrodes and stays in the field of view of the camera. For the cantilever deflection method, we linearly increase the DC voltage from 0 to 2000 V over 8 s.

In both setups, a Phantom VEO-E 310 L camera (set to record at 6000 fps at 1024 × 500 pixel, 10 µs exposure time) with a microscope lens (5x/0.15 A, LU Plan, Nikon) records a profile view of the 2.5 mm diameter droplet. Facilitated by silhouette lighting (see Supporting Information: Figure S4), image processing (in Python using the open-cv library[54]) is used to extract the droplet contour and the cantilever deflection. The droplet contour detection is used to calculate the left and right contact angles and the center of the mass for the free acceleration method. To calculate the center of mass, we assume that the droplet shape that protrudes in and out of the image plane is curved like a sphere. Consequently, we estimate the droplet volume by revolving the contour around the horizontal axis and then determine the center of this volume. Throughout our experiments, the right contact angle is the front/advancing contact angle, and the left contact angle is the rear/receding contact angle. The drop velocity is estimated using the smooth noise-robust differentiator by Holoborodko.[55]

Apart from the qualitative example figures, each data point has been measured at least three times with different samples, and the mean and standard error are plotted. We switch out both the droplet and the sample (dielectric layer and electrodes) after each experiment, using magnetic contacts for rapid sample exchanges (see Supporting Information: Figure S4). If we only switch out the droplet and not the sample, the new droplet is influenced by the previous experiment on that sample. The sample likely retains residual charges in the dielectric layer, which attract a new droplet even if all electrodes and the droplet are grounded.

ACKNOWLEDGMENTS

This work was supported by the Swiss National Science Foundation (SNSF) under grant No. 200020_184661. The authors thank Giulio Grasso, Dr. Florian Hartmann, and Dr. Michael Smith for helpful discussions and support on experimental setups.

CONFLICT OF INTEREST STATEMENT

The authors declare no conflict of interest.

ORCID

Robert Hennig http://orcid.org/0000-0002-8322-5605
Vito Cacucciolo https://orcid.org/0000-0001-6411-8698
Herbert Shea http://orcid.org/0000-0003-3527-3036

REFERENCES

1. Berge B, Peseux J. Variable focal lens controlled by an external voltage: an application of electrowetting. *Eur Phys J E*. 2000;3:159-163.
2. Li J, Kim C-J. Current commercialization status of electrowetting-on-dielectric (EWOD) digital microfluidics. *Lab Chip*. 2020;20:1705-1712.
3. Nelson WC, Kim C-J. Droplet actuation by electrowetting-on-dielectric (EWOD): a review. *J Adhes Sci Technol*. 2012;26:1747-1771.
4. Darhuber AA, Troian SM. Principles of microfluidic actuation by modulation of surface stresses. *Annu Rev Fluid Mech*. 2005;37:425-455.
5. Cho SK, Moon H, Kim C-J. Creating, transporting, cutting, and merging liquid droplets by electrowetting-based actuation for digital microfluidic circuits. *J Microelectromech Syst*. 2003;12:70-80.
6. Umapathi U, Chin S, Shin P, Koutentakis D, Ishii H. Scaling electrowetting with printed circuit boards for large area droplet manipulation. *MRS Adv*. 2018;3:1475-1483.
7. Pollack MG, Fair RB, Shenderov AD. Electrowetting-based actuation of liquid droplets for microfluidic applications. *Appl Phys Lett*. 2000;77:1725-1726.
8. Hines L, Petersen K, Lum GZ, Sitti M. Soft actuators for small-scale robotics. *Adv Mater*. 2017;29:1603483.
9. Barth CA, Hu X, Mibus MA, Reed ML, Knospe CR. Large membrane deflection via capillary force actuation. *J Micromech Microeng*. 2018;28:065008.
10. Takei A. Capillary micro motor. In: Lambert P, ed. *Surface Tension in Microsystems. Microtechnology and MEMS*. Springer; 2013:199-209.
11. Colgate E, Matsumoto H. An investigation of electrowetting-based microactuation. *J Vac Sci Technol, A*. 1990;8:3625-3633.
12. Jenkins J, Kim C-J. Generation of pressure by ewod-actuated droplets. *Solid-State Sensors, Actuators, and Microsystems Workshop*, Hilton Head Island, South Carolina, USA, 2012:145-148.
13. Kedzierski J, Holihan E. Linear and rotational microhydraulic actuators driven by electrowetting. *Sci Robot*. 2018;3:eaat5643.
14. Kedzierski J, Chea H. Multilayer microhydraulic actuators with speed and force configurations. *Microsyst Nanoeng*. 2021;7:22.
15. Wang K-L, Jones TB. Saturation effects in dynamic electrowetting. *Appl Phys Lett*. 2005;86:054104.
16. Ni Q, Capecci DE, Crane NB. Electrowetting force and velocity dependence on fluid surface energy. *Microfluid Nanofluid*. 2015;19:181-189.
17. Mugele FG, Baret J-C. Electrowetting: from basics to applications. *J Phys Condens Matter*. 2005;17:R705-R774.
18. Mugele F. Fundamental challenges in electrowetting: from equilibrium shapes to contact angle saturation and drop dynamics. *Soft Matter*. 2009;5:3377-3384.
19. Berthier J. Electrowetting theory. In: *Micro-Drops and Digital Microfluidics*. Elsevier; 2013:161-224.
20. Wu H, Dey R, Siretanu I, et al. Electrically controlled localized charge trapping at amorphous fluoropolymer–electrolyte interfaces. *Small*. 2020;16:1905726.
21. Li X, Tian H, Shao J, et al. Decreasing the saturated contact angle in electrowetting-on-dielectrics by controlling the charge trapping at liquid-solid interfaces. *Adv Funct Mater*. 2016;26:2994-3002.
22. Verheijen HJJ, Prins MWJ. Reversible electrowetting and trapping of charge: model and experiments. *Langmuir*. 1999;15:6616-6620.

23. Drygiannakis AI, Papathanasiou AG, Boudouvis AG. On the connection between dielectric breakdown strength, trapping of charge, and contact angle saturation in electrowetting. *Langmuir*. 2009;25:147-152.
24. Vallet M, Vallade M, Berge B. Limiting phenomena for the spreading of water on polymer films by electrowetting. *Eur Phys J B*. 1999;11:583-591.
25. James AJ, Vukasinovic B, Smith MK, Glezer A. Vibration-induced drop atomization and bursting. *J Fluid Mech*. 2003;476:1-28.
26. Gu H, Malloggi F, Vanapalli SA, Mugele F. Electrowetting-enhanced microfluidic device for drop generation. *Appl Phys Lett*. 2008;93:183507.
27. Mugele F, Buehrle J. Equilibrium drop surface profiles in electric fields. *J Phys Condens Matter*. 2007;19:375112.
28. Jones TB. An electromechanical interpretation of electrowetting. *J Micromech Microeng*. 2005;15:1184-1187.
29. Chen L, Bonaccurso E. Electrowetting—from statics to dynamics. *Adv Colloid Interface Sci*. 2014;210:2-12.
30. Jones TB. More about the electromechanics of electrowetting. *Mech Res Commun*. 2009;36:2-9.
31. Wang K-L, Jones TB. Electrowetting dynamics of microfluidic actuation. *Langmuir*. 2005;21:4211-4217.
32. Jones TB, Wang K-L, Yao D-J. Frequency-dependent electromechanics of aqueous liquids: electrowetting and dielectrophoresis. *Langmuir*. 2004;20:2813-2818.
33. Crane NB, Mishra P, Volinsky AA. Characterization of electrowetting processes through force measurements. *Rev Sci Instrum*. 2010;81:043902.
34. Semprebon C, Brinkmann M. On the onset of motion of sliding drops. *Soft Matter*. 2014;10:3325.
35. Gupta R, Sheth DM, Boone TK, Sevilla AB, Fréchette J. Impact of pinning of the triple contact line on electrowetting performance. *Langmuir*. 2011;27:14923-14929.
36. Zeng J, Korsmeyer T. Principles of droplet electrohydrodynamics for lab-on-a-chip. *Lab Chip*. 2004;4:265-277.
37. Vo Q, Su H, Tran T. Universal transient dynamics of electrowetting droplets. *Sci Rep*. 2018;8:836.
38. Annapragada SR, Dash S, Garimella SV, Murthy JY. Dynamics of droplet motion under electrowetting actuation. *Langmuir*. 2011;27:8198-8204.
39. Vo Q, Tran T. Contact line friction of electrowetting actuated viscous droplets. *Phys Rev E*. 2018;97:063101.
40. Vo Q, Tran T. Dynamics of droplets under electrowetting effect with voltages exceeding the contact angle saturation threshold. *J Fluid Mech*. 2021;925:A19.
41. Lee SJ, Lee S, Kang KH. Droplet jumping by electrowetting and its application to the three-dimensional digital microfluidics. *Appl Phys Lett*. 2012;100:081604.
42. Burkhart CT, Maki KL, Schertzer MJ. Coplanar electrowetting-induced droplet detachment from radially symmetric electrodes. *Langmuir*. 2020;36:8129-8136.
43. Vo Q, Tran T. Critical conditions for jumping droplets. *Phys Rev Lett*. 2019;123:024502.
44. Wei Q, Yao W, Gu L, et al. Modeling, simulation, and optimization of electrowetting-on-dielectric (EWOD) devices. *Biomicrofluidics*. 2021;15:014107.
45. Wang W, Rui X, Sheng W, et al. An asymmetric electrode for directional droplet motion on digital microfluidic platforms. *Sens Actuators, B. Chem*. 2020;324:128763.
46. Eral HB, 't Mannetje DJCM, Oh JM. Contact angle hysteresis: a review of fundamentals and applications. *Colloid Polym Sci*. 2013;291:247-260.
47. Lu H-W, Glasner K, Bertozzi AL, Kim C-J. A diffuse-interface model for electrowetting drops in a Hele-Shaw cell. *J Fluid Mech*. 2007;590:411-435.
48. Sen P, Kim C-J. A fast liquid-metal droplet microswitch using EWOD-driven contact-line sliding. *J Microelectromech Syst*. 2009;18:174-185.
49. Kang KH. How electrostatic fields change contact angle in electrowetting. *Langmuir*. 2002;18:10318-10322.
50. Mugele F, Herminghaus S. Electrostatic stabilization of fluid microstructures. *Appl Phys Lett*. 2002;81:2303-2305.
51. Du J, Chamakos NT, Papathanasiou AG, Min Q. Initial spreading dynamics of a liquid droplet: the effects of wettability, liquid properties, and substrate topography. *Phys Fluids*. 2021;33:042118.
52. Piezotech. Technical Guide Piezotech RT-TS. 2020.
53. Gao N, Geyer F, Pilat DW, et al. How drops start sliding over solid surfaces. *Nat Phys*. 2018;14:191-196.
54. Bradski G. The openCV library. *Dobbs J Softw Tools Prof Program*. 2000;25:120-123.
55. Holoborodko P. Smooth noise robust differentiators. Published online, 2008. http://www.holoborodko.com/pavel/numerical-methods/numerical-derivative/smooth-low-noise-differentiators/

SUPPORTING INFORMATION

Additional supporting information can be found online in the Supporting Information section at the end of this article.

How to cite this article: Hennig R, Cacucciolo V, Shea H. Actuating droplets with electrowetting: force and dynamics. *Droplet*. 2024;3:e108. doi:10.1002/dro2.108